Electrical and structural properties of nanoscale NiSi$_2$ precipitates in silicon

F. Riedel* and W. Schröter

Georg-August-Universität Göttingen, IV. Physikalisches Institut, Bunsenstrasse 13-15, D-37073 Göttingen, Germany
(Received 5 May 2000)

Structurally well-defined NiSi$_2$ platelets of two {111}-silicide lattice planes thickness and 37 nm diameter form after in-diffusion of nickel in *n*-type silicon at 900 °C followed by rapid quenching. These platelets are bounded by a dislocation ring and exhibit in deep-level-transient-spectroscopy (DLTS) measurements a line that can be attributed to bandlike electronic states at the extended defect. We exploit internal ripening of individual precipitates upon additional annealing at 320 °C in order to study the temporal evolution of their electrical and structural properties. Within a short time of about 1 min one observes a continuous transmutation of DLTS line characteristics, finally revealing localized states at the defect. Structural changes towards a compact shape become observable by means of transmission electron microscopy on a significantly larger time scale of several minutes. We conclude that the bounding dislocation ring determines the electrical activity of platelets as-quenched. Due to its particular core structure, the dislocation exhibits characteristics of a quantum wire. A specific core defect that allows us to construct curved dislocation line segments causes meandering, which has been shown to be the weakest perturbation of ideal one-dimensional behavior.

I. INTRODUCTION

Silicide platelets of cobalt,[1] nickel,[2] and copper[3] in silicon, as obtained by fast quenching from high diffusion temperatures,[4] are expected to exhibit unique structural and electrical properties.[5,6] In the case of nickel, it has been shown that NiSi$_2$ platelets consisting of two {111} atomic layers of silicide are adjustable in diameter between 10 nm and 0.9 μm.[2,7,8] These platelets are bounded by a dislocation ring, strictly running in the platelet plane and associated with a wide core.[9] Due to their small size, the platelets are supposed to show the characteristics of a quantum dot or, if the dislocation ring is dominating the electrical activity, that of a quantum wire ring.

Deep-level transient spectroscopy[10] (DLTS) has shown that a wide distribution of deep electronic states in the band gap of silicon is associated with the platelets.[7,11] The energy spectrum of these states is quite different from those associated with defect states at glide dislocations in Si.[12,13] From modeling and numerical simulations, it has been concluded that electron equilibration is fast ($<10^{-5}$ s) at the platelets and slow ($>10^{-1}$ s) at glide dislocations.[14] It remained open which structural unit of the platelet—the NiSi$_2$/Si interface or the dislocation ring—is the electrically active one. In this work, we demonstrate combining DLTS and high-resolution transmission electron microscopy (HRTEM), the result being that the dislocation ring determines the electrical activity of the platelets as-quenched. Hence, the bounding dislocation loops are expected to show properties of quantum wire systems.

Other semiconductor quantum wire systems are usually fabricated by the cleaved edge overgrowth technique[15] or molecular-beam epitaxy on vicinal surfaces[16] of III-V compound semiconductors, or as carbon nanotubes.[17] Recently, such structures have been used to evidence Luttinger liquid behavior of one-dimensional (1D) systems.[18] By means of resonant-tunneling experiments, the power-law drop of the density of states at the Fermi level, a specific feature of Luttinger liquids, has been verified.[19] Elastic scattering in 1D systems is expected to occur by the short-range part of the scattering potential since an electron in state k can only reach state $-k$. High 1D mobility values have been predicted,[20] but this prediction neglected the fact that even small perturbations significantly affect the 1D electronic ground state. Compositional disorder in III-V heterostructures induces meandering, edge fluctuations of the wire, and island formation within the wire.[21,22] This leads to increasing deviation from ideal 1D behavior.

For the system studied in this work, we investigate the impact of structural disturbances on electronic structure. Since NiSi$_2$ platelets are found even after the fastest quench (2000 K/s), their dislocation ring is presumably undecorated. The core structure proposed below to construct the curved dislocation line causes meandering, which has been shown to be the weakest perturbation of the 1D electronic system.[22] By means of additional annealing at moderate temperature, the NiSi$_2$ platelet structure, which is a kinetically determined metastable precipitate configuration,[9] can be modified. The bounding dislocation loop is then subjected to local structural changes. This should be reflected by a destruction of quantum ring characteristics.

This paper is organized as follows. After the Introduction, a brief description of experimental details is given. Section III first shows HRTEM and DLTS investigations on nanoscale NiSi$_2$ platelets as-quenched, which exhibit bandlike electronic states. Then the temporal evolution of electrical and structural properties upon additional annealing is presented. DLTS reveals the transition to localized states, whereas by means of HRTEM, internal ripening of precipitates is documented. Finally, the results are discussed in view of quantum wire behavior. From balls-and-sticks modeling we find that the core defect, responsible for the curvature of the dislocation ring, causes meandering as the weakest perturbation of the 1D electronic system.

II. EXPERIMENTAL DETAILS

For in-diffusion, nickel was evaporated on FZ Si samples cut from (001) oriented wafers, doped with 1.4 $\times 10^{15}$ P atoms/cm^3. Samples sizes amounted to 10×10

$\times 0.8$ mm^3. The heat treatment to saturate Si with nickel at 900 °C was performed in a vertical furnace in ambient Ar. Annealing was finished by quenching the sample to room temperature in 10% NaOH (estimated quench rate $-\dot{T}$ ≈ 2000 K/s).

After mechanically removing about 100 μm from each surface, gold was evaporated as a Schottky contact on a finally chemomechanically polished surface for DLTS measurements. The spectra were recorded at reverse bias U_B $=4$ V and pulse voltage $U_P=4$ V. Measurement frequency f_m was 68 Hz. Following the filling pulse of length t_p, the capacitance transient was recorded with a delay time t_d of 50 μs. Note that the ordinate in the spectra presents the value of the normalized capacitance transient correlated with a rectangular function according to the lock-in amplifier we used (PAR model 129), i.e.,

$$S_{\text{DLTS}} \equiv \frac{1}{T_m} \left\{ \int_{t_d}^{(t_d/2)+(T_m/2)} \frac{C_0 - C(t)}{C_0} dt \right.$$

$$\left. - \int_{(t_d/2)+(T_m/2)}^{T_m} \frac{C_0 - C(t)}{C_0} dt \right\}.$$

$T_m = 1/f_m$ denotes the correlation period, C_0 the capacitance of the Schottky contact under reverse bias, $C_0 - C(t)$ the capacitance transient, and S_{DLTS} denotes the DLTS signal.

For TEM investigations, cross-section foils in $\langle 110 \rangle$ orientation were prepared by a combination of mechanical thinning and ion milling at liquid nitrogen temperature. Convergent beam electron diffraction,[23,24] conventional TEM (determination of precipitate density), and five-beam lattice images in $\langle 110 \rangle$ projection were recorded at 120 kV in a Philips 420 ST with a point resolution of 0.30 nm.

Rapid thermal annealing in a tungsten lamp furnace (model NANOSIL RTP 600 from Modular Process Technology) in Ar atmosphere at 320 °C was applied for times ranging from 10 s to 12 min. A long-time anneal for 20 h was performed in a conventional furnace. Subsequently, each specimen was characterized by DLTS. Selected ones were investigated by TEM.

III. RESULTS

A. Bandlike states

Figure 1 shows a lattice image of a typical disk-shaped precipitate lying on Si($1\bar{1}1$) lattice planes obtained after quenching in 10% NaOH from 900 °C. The darker appearance of the particle compared with the silicon matrix is due to the change in extinction lengths according to the change in chemical composition. It is restricted to two {111} layers. A displacement of the silicon lattice on top of the precipitate with respect to that at the bottom is indicated in the enlarged part of Fig. 1 by a line along $[\bar{1}10]$. The projection of this displacement onto the (110) plane is $a/4[001]$, pointing away from the particle. The latter can be shown by measuring the distance of three {111} planes including the platelet giving 1.01 nm compared with 0.94 nm for silicon and NiSi$_2$. These observations are in full agreement with the description of NiSi$_2$ platelets obtained after quenching in ethylene glycol (estimated quench rate $-\dot{T} \approx 1000$ K/s) as given
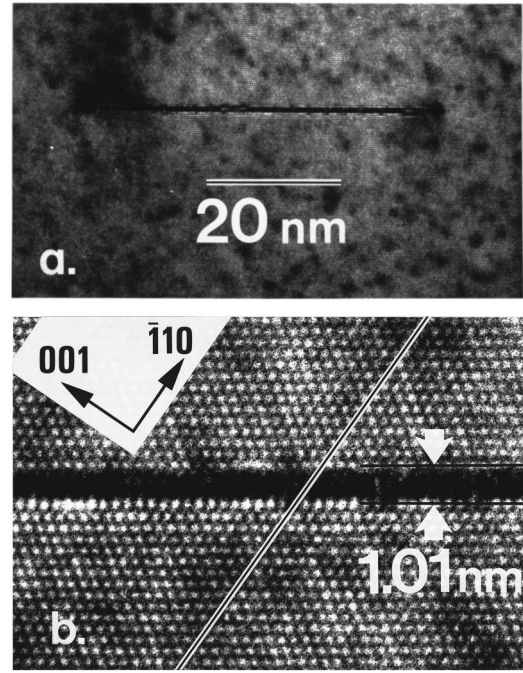

FIG. 1. (a) HRTEM lattice image of a typical disk-shaped NiSi$_2$ precipitate lying on Si($1\bar{1}1$) lattice planes obtained after quenching in 10% NaOH from diffusion temperature 900 °C. The dark appearance of the particle compared with the Si matrix is due to the change in chemical composition. (b) Enlarged part of (a) showing the displacement of the silicon lattice indicated by the line along $[\bar{1}10]$; note that the distance of three ($1\bar{1}1$) lattice planes including the particle is 1.01 nm compared to 0.94 nm for silicon and NiSi$_2$.

by Seibt and Schröter.[2] Hence, under our experimental conditions yielding platelet diameters by an order of magnitude smaller, we have the same atomic structure: coherent platelets consisting of two NiSi$_2$ {111} layers in type-A orientation, i.e., they have the same orientation as the Si matrix. Their interface to the silicon matrix is formed by Si-Si bonds. The platelets are metastable, since the nickel atoms are sevenfold coordinated instead of eightfold in bulk NiSi$_2$. Associated with this interfacial structure is a dislocation bounding the precipitate, which has a Burgers vector $a/4\langle 111 \rangle$ inclined with respect to the platelet normal ($a = 0.543$ nm lattice constant of Si).

The volume density N_V of the precipitates amounts to $(4.5 \pm 0.8) \times 10^{12}$ cm^{-3}. TEM examinations showed no systematic variation of particle density with sample depth after removal of about 100 μm from each surface. The mean diameter d of the NiSi$_2$ platelets is (37 ± 6) nm. We want to mention that it is possible to vary the NiSi$_2$-platelet diameter d between about 10 and 900 nm by variation of diffusion temperature between 750 and 1050 °C and variation of quenching rate $-\dot{T}$.[2,7,8]

Recently, it has been demonstrated that DLTS of spatially extended defects, when compared to DLTS of point defects, is significantly affected by the complex interplay of three parameters, as shown in Fig. 2:[14] the capture barrier, which varies with the defect charge and modifies the capture rate; the density of states, which leads to line broadening; and the internal equilibration time Γ_i of the electron distribution at
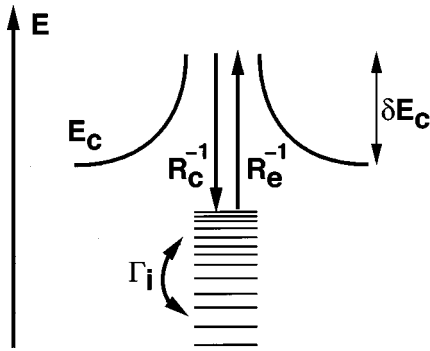
FIG. 2. Band diagram of electronic states at an extended defect. Shown is the capture barrier δE_c resulting from defect occupation larger than the occupation of the neutral defect. The internal equilibration time Γ_i allows us to classify deep states as *bandlike* ($\Gamma_i \ll R_e^{-1}, R_c^{-1}$) or *localized* ($\Gamma_i \gg R_e^{-1}, R_c^{-1}$), where R_e and R_c denote the emission and capture rate, respectively.

the defect, which determines the filling pulse dependence of the line shape. When compared to the inverse carrier emission rate R_e^{-1} and capture rate R_c^{-1}, the internal equilibration time allows us to distinguish between *bandlike* ($\Gamma_i \ll R_e^{-1}, R_c^{-1}$) and *localized* ($\Gamma_i \gg R_e^{-1}, R_c^{-1}$) states.

In the case of bandlike states, variation of filling pulse length t_p results in broadened DLTS lines whose maximum shifts towards lower temperature with increasing t_p and whose high-temperature sides coincide.[14,25] In contrast, for localized states the DLTS line maximum stays constant, whereas line amplitudes and high-temperature sides of the different asymmetrically broadened lines exhibit specific dependence on t_p over a wide range, the so-called logarithmic capture law, i.e., $\Delta C/C_0 \sim \log_{10} t_p$. This has been shown to be valid for any distribution of levels at an extended defect and can be seen as criteria to distinguish localized from bandlike states by means of DLTS measurement.[14,26]

Samples containing NiSi$_2$ platelets as-quenched exhibit a broad DLTS line, which was observed neither in as-grown nor in control samples annealed without nickel. In accordance with the TEM examinations revealing constant particle density, all samples exhibited this DLTS line with an amplitude $\Delta C_{max}/C_0$ of $(8\pm4)\times10^{-3}$. Figure 3 shows the result of a variation of filling pulse length t_p, i.e., a study of the capture behavior. The high-temperature sides of the lines are mainly independent of t_p and the maximum temperature of the lines decreases with increasing t_p. Applying the above
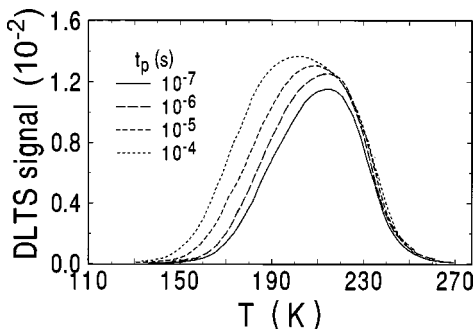
TABLE I. Volume density N_V of NiSi$_2$ precipitates after quenching from diffusion temperature of 900 °C and subsequent annealing at 320 °C. The statistical error for N_V is mentioned. The error resulting from determination of TEM foil thickness by means of convergent electron beam diffraction contributes about 10%. Within the limit of error the particle density remains constant.

State	N_V (10^{12} cm^{-3})
as-quenched	4.5 ± 0.8
320 °C, 300 s	4.5 ± 1.5
320 °C, 720 s	5.1 ± 1.1
320 °C, 20 h	5.3 ± 0.6

criteria, we conclude that NiSi$_2$ platelets in n-Si as-quenched are associated with bandlike states. This identification also holds when electric-field-enhanced emission as well as minority carrier emission is taken into account.[25]

B. Localized states

On annealing at a temperature of 320 °C, the volume density N_V of particles remains constant as can be seen from Table I. To achieve a decrease in N_V due to Ostwald ripening requires additional annealing between 500 and 900 °C.[2]

We observe a significant change of DLTS line characteristics within only a few minutes of annealing. Figure 4 shows the temporal evolution of the DLTS line at filling pulse length $t_p = 100$ μs. For better comparison, the different spectra are normalized to their maximum amplitude. The whole line continuously shifts towards higher temperatures. If one chooses T_{max}, the temperature of the DLTS line maximum, as the parameter to seize this development, it becomes clear that the main fraction of the line shift occurs during about the first minute. This is followed by a further slight shift on a larger time scale. In a plot of T_{max} versus annealing time t, linear extrapolation for the respective time regime results in a "transition" time of about 30 s, defined from the intersection of the two extrapolated lines, after which the main evolution is completed. We also performed annealings of 10 s duration at various temperatures ranging from 140 to 290 °C.
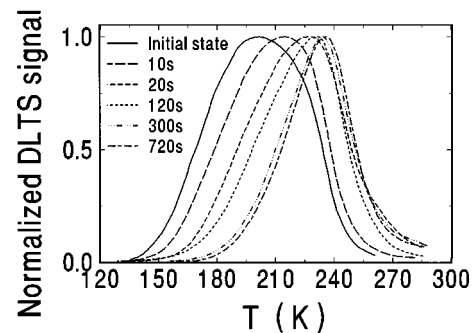

FIG. 3. DLTS line associated with NiSi$_2$ platelets as-quenched (cf. Fig. 1) and its dependence on filling pulse length t_p exhibiting bandlike states at the extended defect.

FIG. 4. Temporal evolution of the DLTS line associated with NiSi$_2$ precipitates during additional annealing at 320 °C. For better comparison the different spectra ($t_p = 100$ μs) are normalized. The whole line continuously shifts towards higher temperatures and changes its shape. [Peak value of the respective DLTS signal: 6.1 $\times10^{-3}$ (initial state); 8.9×10^{-3} (annealing time 10 s); 8.2×10^{-3} (20 s); 9.4×10^{-3} (120 s); 8.0×10^{-3} (300 s); 6.3×10^{-3} (720 s).]
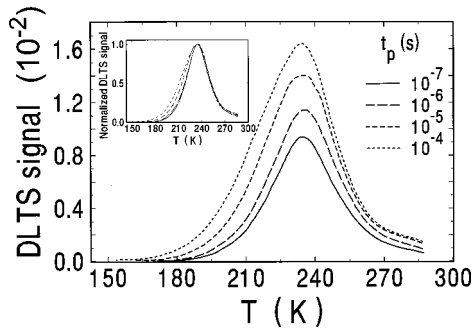
FIG. 5. DLTS line associated with NiSi$_2$ precipitates after additional annealing at 320 °C for 5 min when the main evolution of electrical properties is completed. Compared to the initial DLTS line (Fig. 3) the entire characteristics changed, revealing localized states at the extended defect.

Even for the lowest temperature, the DLTS signal is already modified compared to the initial state as-quenched and exhibits a small shift of T_{max}.

Figure 5 presents the result of t_p variation after annealing for 5 min, when the main temporal evolution of the DLTS line is completed. Compared to the initial DLTS line (Fig. 3), the entire characteristics has changed but is still completely different from a DLTS line associated with point defects. According to the criteria mentioned above, the DLTS line now reveals localized states at the extended defect. The line is asymmetrically broadened. High-temperature sides coincide after normalization as shown in the inset. Variation of line amplitude with t_p is more pronounced than in the initial state and obeys a logarithmic capture law, i.e., $\Delta C/C_0 \sim \log_{10} t_p$. The dependence of T_{max} on t_p almost vanished, as can be seen from Fig. 6, where the slopes $|dT_{max}/d\log_{10} t_p|$ resulting from t_p variation for the respective specimen are shown versus annealing time. Again, one notes that after the first minute the dependence is strongly reduced.

In accordance with the TEM result of constant precipitate density N_V, the DLTS line amplitude $\Delta C_{max}/C_0$ does not decrease with annealing time, but remains within the range of $(8\pm4)\times10^{-3}$ (cf. Fig. 4).

After several minutes annealing, a change of particle shape becomes observable by means of HRTEM. In samples annealed up to 2 min, structural changes of platelets were not yet detectable. Hence, Figs. 7 and 8 show lattice images of NiSi$_2$ precipitates after annealing for 5 and 12 min, respec-
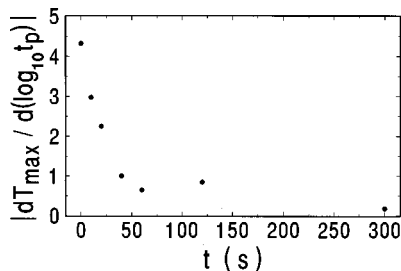

FIG. 6. Slope $|dT_{max}/d\log_{10} t_p|$ resulting from the respective DLTS filling pulse length variation versus annealing time t. The dependence of T_{max} on t_p is strongly reduced within the first minute.
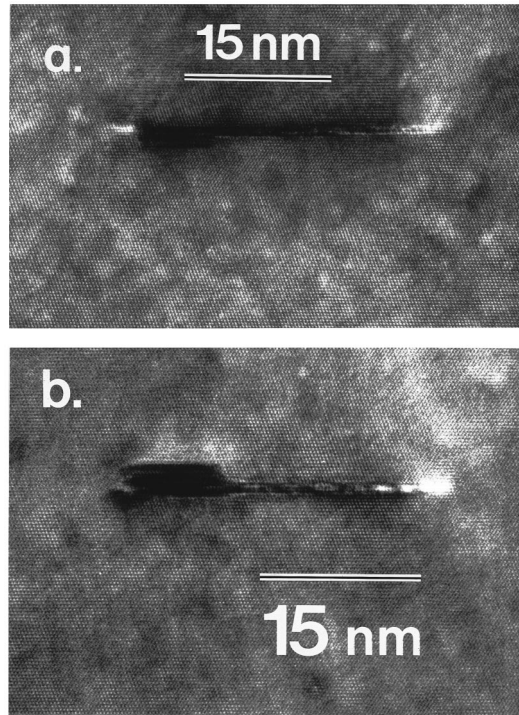

FIG. 7. Lattice images of typical NiSi$_2$ precipitates after additional annealing at 320 °C for 5 min. One observes the formation of small islands which have crystallographically well-defined shapes leading to steps in the NiSi$_2$-Si interface of three (a) or six (b) interplanar {111} distances in height.

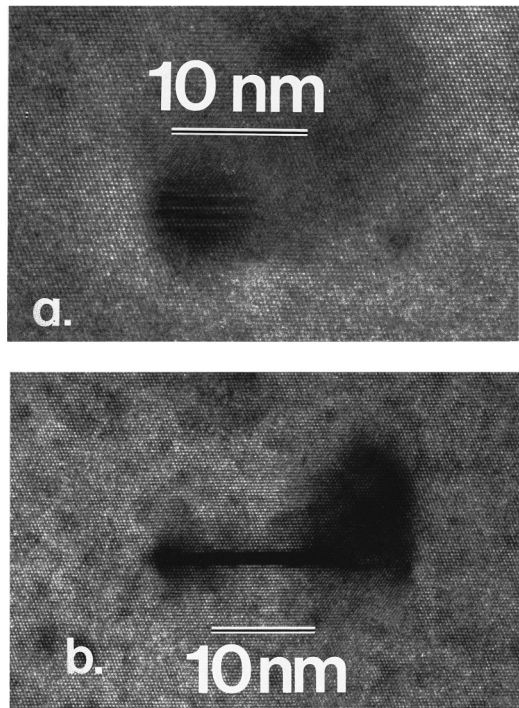FIG. 8. Lattice images of NiSi$_2$ precipitates after additional annealing at 320 °C for 12 min. (a) Moiré pattern indicates twin orientation of the ripened particle with respect to the silicon matrix (type-B orientation). (b) A precipitate with orientation of type-A which is three NiSi$_2${111} layers thick.

tively. One observes a change from disk-shaped (Fig. 1) to a more compact form. This ripening process of individual particles has been termed internal ripening.[7,11] The thickness increases while the diameter decreases. This proceeds via local formation of islands at the border of the platelet, which have crystallographically well-defined shapes with steps in the $NiSi_2$-Si interface of three or six interplanar {111} distances in height [Figs. 7(a) and 7(b)]. The Moiré pattern provides evidence for twin orientation of growing islands or ripened particles [Fig. 8(a)] with respect to the silicon matrix (type-*B* orientation). Other ripened particles of, e.g., three $NiSi_2${111} layers thickness [Fig. 8(b)] exhibit type-*A* orientation. The finding is in agreement with a recent theoretical calculation on the stability of these two different interface structures. It was shown that the interface structure with the lowest energy changes from type-*A* for two $NiSi_2${111} layers to type-*B* for at least five layers thickness.[27]

IV. DISCUSSION

Our main result states that on annealing, the electronic structure of $NiSi_2$ platelets undergoes a significant change before modifications of the platelet's singular shape become detectable by means of HRTEM. We take this finding as evidence that it is the bounding dislocation ring that originates the observed electrical activity of the platelet. It is well known that the electronic ground state of 1D systems is sensitively dependent on perturbations caused by defects.[28] On annealing, the dislocation movement is most probably the first step of the platelet's structural relaxation. We shall argue below that bandlike electronic states are possible for the dislocation ring if it is running strictly in the platelet plane. Any deviation out of this plane is then expected to be a major perturbation of the dislocation core and of its electronic ground state. Indeed, our second result states that as soon as structural changes of the platelet become detectable, the electronic states have changed from bandlike to localized.

What might be the reason that the platelet's bounding dislocation initially exhibits deep bandlike states as opposed to, e.g., 30° or 90° glide-set partial dislocations in Si, which in their energetically favorable reconstructed core configurations do not provide any deep electron level in the band gap?[29] The dislocation bounding the platelet has a possible core structure, presented in Fig. 9(a), which is rather different from that of dislocations generated by plastic deformation of Si.[9] The core does not contain Si dangling bonds but rather two Ni atoms with deficient coordination, one with fourfold and the other with sixfold coordination instead of eightfold as in bulk $NiSi_2$. Theoretical investigations on a single $NiSi_2$ layer buried in bulk Si have shown that Ni atoms with deficient coordination provide deep bands in the band gap.[30] Hence, the specific core configuration of the bounding dislocation ring becomes a prerequisite to observe bandlike states.

To construct a curved dislocation line in the {111} plane of the platelet, the three possible ⟨110⟩ segments must be joined by a link, whose possible structure is shown in Figs. 9(b) and 9(c) (plan view of the upper and lower platelet plane). It differs from the core structure of ⟨110⟩ segments only by a larger coordination of one Ni atom. The number

(a)
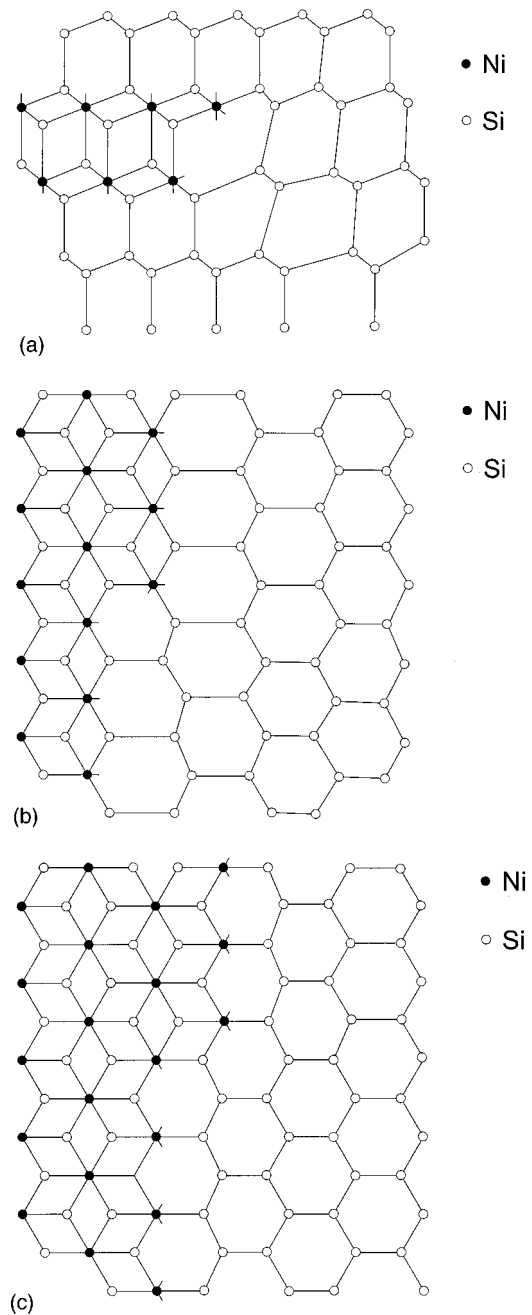
• Ni
○ Si

(b)

• Ni
○ Si

(c)

• Ni
○ Si

FIG. 9. (a) Model of the possible core structure of a $b=a/4\langle 111 \rangle$ dislocation bounding the platelet. The core does not contain Si dangling bonds but Ni atoms with deficient coordination (fourfold and sixfold, respectively, instead of eightfold as in bulk $NiSi_2$) [after Seibt and Schröter (Ref. 9)]. (b),(c) Possible structure of the elementary link which allows us to construct a curved dislocation line in the {111} plane of the $NiSi_2$ platelet. Plan view of the upper (b) and the lower (c) platelet plane. It differs from the core structure shown in (a) only by a larger coordination of one Ni atom. Number and coordination of Si atoms remain unchanged. Periodicity and back bonds of line segments remain undisturbed.

and coordination of the Si atoms are unchanged. Periodicity and back bonds of line segments remain undisturbed. Due to the strict flatness of the platelet, the complete dislocation loop can be constructed with these joined segments, avoiding the occurrence of kinks or jogs.

How does this affect the energy spectrum of the disloca-

tion? Taylor *et al.*[21] and later Nicolić and MacKinnon[22] used the tight-binding method to study the influence of compositional disorder on the electronic density of states and localization lengths of quantum wires. Taking into account meandering (variation of wire center position but constant width), edge fluctuations (additionally variation of width) of the wire, and island structures within the wire yield increasing impact.

The density of states of an ideal one-dimensional system has a minimum at the center ($E=0$) and $1/\sqrt{E}$ singularities at band edges. Meandering as the weakest perturbation and in our case presumably reproducing approximately the curvature of the bounding dislocation loop leads to suppression of the band-edge singularities and to a sharp dip of the density of states with a narrow band gap and a spike at $E=0$. The origin of band gap and spike has been discussed in some detail by Kirkpatrick and Eggarter.[31] Molecular states that are localized partially by interference and partially by the defects linking the dislocation segments give rise to it. Concerning the extension of electronic states, it has been proven that the elements of the transmission matrix for a long disordered wire show an asymptotic exponential decrease with L, the length of the wire.[28,32] The localization length shows opposite trends in its variation with energy as the density of states. For a meandering wire, localization of all states within about 70 lattice spacings results except in the vicinity of the band edges.[22] This value is close to the diameter of the dislocation loop studied in this work, so that the analogy between dislocation loop and meandering wire results in a plausible explanation for the *bandlike* characteristics of the DLTS signal, which we associate with the dislocation bounding the NiSi$_2$ platelets obtained after quenching.

Internal ripening requires a rearrangement of Ni and Si atoms. Detachment of Ni atoms might be facilitated in the core of the dislocation bounding the platelet. The meandering dislocation loop configuration, responsible for initial quantum ring behavior, becomes disturbed since the platelets' structural relaxation leads to a deviation from its strictly planar configuration. DLTS reveals this process as a rapid change of the electronic structure, whereas structural changes by means of TEM become observable on a larger time scale.

We want to mention that recently, by means of resonant-tunneling experiments, features of a Luttinger liquid have been shown to exist for other semiconductor quantum wire structures.[18,19] This method requires electrical contacts, which up to now have not been available for the NiSi$_2$ platelets studied in this work. However, the platelets couple to microwave fields, so that measurements of conductance should become possible.[33] From such measurements one can determine 1D electron mobility values of the bounding dislocation ring.

In summary, we presented in this work experimental results on electrical and structural properties of nanoscale NiSi$_2$ precipitates in silicon. After rapid quenching, platelets which are two {111}-silicide lattice planes thin and 37 nm in diameter exhibit bandlike electronic states. These states are associated with the dislocation ring bounding the platelet, which was discussed in view of meandering quantum wire behavior. We studied in detail the evolution of electrical properties towards localized states at the extended defect upon additional annealing at 320 °C. This occurs on a significantly shorter time scale than the structural changes of internal ripening observed by means of HRTEM.

ACKNOWLEDGMENT

---

*Corresponding author. Email: riedel@ph4.physik.uni-goettingen.de, FAX: +49-551-394574.

[1] J. Utzig, J. Appl. Phys. **64**, 3629 (1988).

[2] M. Seibt and W. Schröter, Philos. Mag. A **59**, 337 (1989).

[3] M. Seibt, in *Semiconductor Silicon–1990*, edited by H. R. Huff, K. G. Barraclough, and J.-I. Chikawa (The Electrochemical Society, Pennington, NJ, 1990), p. 663.

[4] W. Schröter, M. Seibt, and D. Gilles, in Handbook on Semiconductor Technology, edited by W. Schröter and K. A. Jackson (VCH, Weinheim, 2000), p. 597.

[5] A. A. Istratov and E. R. Weber, Appl. Phys. A: Mater. Sci. Process. **66**, 123 (1998).

[6] M. Seibt, H. Hedemann, A. A. Istratov, F. Riedel, A. Sattler, and W. Schröter, Phys. Status Solidi A **171**, 301 (1999).

[7] U. Gnauert, Diploma thesis, Universitaet of Göttingen, 1990.

[8] F. Riedel, Ph.D. thesis, Universitaet of Göttingen, 1994.

[9] M. Seibt and W. Schröter, Solid State Phenom. **19/20**, 283 (1991).

[10] D. V. Lang, J. Appl. Phys. **45**, 3023 (1974).

[11] F. Riedel, J. Kronewitz, U. Gnauert, M. Seibt, and W. Schröter, Solid State Phenom. **47/48**, 359 (1996).

[12] W. Schröter, I. Queisser, and J. Kronewitz, in *Structure and Properties of Dislocations in Semiconductors 1989*, IOP Conf. Proc. No. 104 (Institute of Physics, London, 1989), p. 75.

[13] D. Cavalcoli, A. Cavallini, and E. Gombia, Phys. Rev. B **56**, 10 208 (1997).

[14] W. Schröter, J. Kronewitz, U. Gnauert, F. Riedel, and M. Seibt, Phys. Rev. B **52**, 13 726 (1995).

[15] A. Yacoby, H. L. Störmer, K. W. Baldwin, L. N. Pfeiffer, and K. N. West, Solid State Commun. **101**, 77 (1997).

[16] J.-S. Lee, H. Isshiki, T. Sugano, and Y. Aoyagi, J. Cryst. Growth **173**, 27 (1997).

[17] M. Bockrath, D. H. Cobden, P. L. McEuen, N. G. Chopra, A. Zettl, A. Thess, and R. E. Smalley, Science **275**, 1922 (1997); S. J. Tans, M. H. Devoret, H. Dai, A. Thess, R. E. Smalley, L. J. Geerligs, and C. Dekker, Nature (London) **386**, 474 (1997).

[18] M. Bockrath, D. H. Cobden, J. Lu, A. G. Rinzler, R. E. Smalley, L. Balents, and P. L. McEuen, Nature (London) **397**, 598 (1999).

[19] O. M. Auslaender, A. Yacoby, R. de Picciotto, K. W. Baldwin, L. N. Pfeiffer, and K. W. West, Phys. Rev. Lett. **84**, 1764 (2000).

[20] H. Sakaki, Jpn. J. Appl. Phys., Part 1 **19**, 94 (1980).

[21] J. P. G. Taylor, K. J. Hugill, D. D. Vvedensky, and A. MacKinnon, Phys. Rev. Lett. **67**, 2359 (1991).

[22] K. Nicolić and A. MacKinnon, Phys. Rev. B **47**, 6555 (1993).

[23] P. M. Kelly, A. Jostsons, R. G. Blake, and J. G. Napier, Phys. Status Solidi A **31**, 771 (1975).

[24] S. M. Allen, Philos. Mag. A **43**, 325 (1981).

[25] H. Hedemann and W. Schröter, Solid State Phenom. **57/58**, 293 (1997).

[26] H. Hedemann and W. Schröter, J. Phys. III **7**, 1389 (1997).

[27] H. Fujitani, Phys. Rev. B **57**, 8801 (1998).

[28] E. Granot, Phys. Rev. B **60**, 10 664 (1999).

[29] For a review, see H. Alexander and H. Teichler, in Handbook on Semiconductor Technology, edited by W. Schröter and K. A. Jackson (VCH, Weinheim, 2000), p. 291 and references therein.

[30] J. T. Schick and S. M. Bose, Phys. Rev. B **53**, 12 609 (1996).

[31] S. Kirkpatrick and T. P. Eggarter, Phys. Rev. B **6**, 3598 (1972).

[32] R. Johnston and H. Kunz, J. Phys. C **16**, 3895 (1983).

[33] V. Kveder (private communication).